The Role of Humidity in Past and Future Fire Weather Trends in the Contiguous United States

Grant Buster,[1a] Tianqi Zhang,[b] Jiafu Mao,[b] Weichen Liu,[c] Stefan Rahimi[c]

[a] Strategic Energy Analysis Center, National Laboratory of the Rockies, Golden, CO 80401, USA

[b] Environmental Sciences Division, Oak Ridge National Laboratory, Oak Ridge, TN 37830, USA

[c] Department of Atmospheric Science, University of Wyoming, Laramie, WY 82071, USA

[1] To whom correspondence may be addressed. Email: Grant.Buster@NLR.gov

Keywords: fire weather, humidity, downscaled data, modelling

This is a non-peer-reviewed preprint submitted to EarthArXiv.

Abstract

There has been evidence of increasing fire activity in the United States since approximately the 1980s, now estimated to cause tens to hundreds of billions of dollars of damage per year. Weather is one of the key drivers of fire activity, with hot, dry, and windy weather commonly associated with high-risk conditions. We are still, however, developing an understanding of how these weather variables have contributed to changing fire weather regimes over the last several decades and whether these changes will continue into the future. In this work, we investigate the effect of declining humidity in arid regions of the United States on fire weather trends. We find that these drying trends have been the predominant contributor to historical increasing trends in fire weather in the Western United States based on a common fire weather index, and that this signal is largely missing from downscaled weather projections based on Earth system models. Accordingly, a near-future (2020–2039) fire weather scenario derived from downscaled Earth System Model data produces little to no change in the frequency of extreme fire weather days across the Western United States. However, under a continued drying scenario, many regions in the West experience 20–70% increases in the annual occurrence of extreme fire weather days.

1 Introduction

Wildfires in the United States have become more common over the last few decades with the Western United States seeing upward trends in burn frequency, burn area, and destroyed

buildings (1, 2). In a 2017 report, the direct monetary annualized costs, which include damages, losses, and fire management costs, were estimated to be between $71 billion and $348 billion in 2016 dollars (3). The United States Congress Joint Economic Committee reported that diminished real estate value and exposure to wildfire smoke are even more costly than property damage alone, estimating total wildfire costs to be between $394 to $893 billion per year (4).

The factors driving these increases in fire risk are numerous and complex. To start, wildland fires are fueled by vegetation, and therefore changes in vegetation drive corresponding changes in wildfire regimes with industrially managed forests being more likely to burn with high severity (5) and invasive grass species increasing fire occurrence by up to 230% (6). However, without a human component, changes in vegetation would not drive changes in societal risk. Between 1945 and 2015, more than 330,000 buildings were added to fire-prone areas (7). The addition of new buildings to wildfire hotspots has increased human exposure to fire risk, especially for low- and intermediate-density settlements in the wildland-urban interface (7). Finally, there is substantial evidence that historical changes in weather and climate, specifically in the warming and drying of the atmosphere over the Western United States, have driven increases in fuel aridity leading to increased burned area (8).

The phenomenon of atmospheric drying over land in the past several decades is well documented, especially for the arid Western United States with concentrations in certain regions of California, Nevada, Utah, Arizona, New Mexico, and Colorado (8, 9). Evidence of this trend can be seen in increasing vapor pressure deficit and decreasing vapor pressure in the fifth major global reanalysis produced by the European Centre for Medium-Range Weather Forecasts (ERA5) and meteorological observation stations from the Integrated Surface Database (9, 10). There are several working theories for the cause of this phenomenon based on atmospheric dynamics and moisture transport (11) and trends in terrestrial evapotranspiration (12). The relevance of these trends with respect to fire weather has been superficially noted, although without quantification of the impact to commonly used fire weather indices or future projections of fire weather (9).

To estimate future changes in fire weather, many have turned to Earth system models (ESMs) (13–15). Projections from ESMs such as those from the Coupled Model Intercomparison Project Phase 6 (CMIP6) are currently the best method to explore possible future fire weather regimes but have noted limitations in their spatial resolution and physical representation of certain fire weather phenomena (16). These ESMs have led to an understanding that rising temperatures will increase risky fire weather, with less confidence in changing patterns of precipitation and other relevant weather variables (16, 17). Crucially, it has been found that the predominant signal for atmospheric moisture over land in virtually all ESM simulations is on average an increase in humidity in the arid and semi-arid regions of the world, contradicting recent observations of drying trends (10). Indeed, others have found that downscaled ESM projections from the Coupled Model Intercomparison Project Phase 5 (CMIP5; now superseded by CMIP6) understate historical trends in fire weather (18). More sophisticated weighted ensembles of ESMs based on fire weather skill can lead to reduced overall bias but are still unable to capture the multidecadal upward trend of fire weather seen in historical reanalysis data (14).

Given the observed decline in atmospheric moisture over arid regions in the United States (9) and the noted absence of these trends in future fire weather projections from ESMs (10), our goal

here is threefold: (1) to quantify the relative importance of these drying trends in historical changes in fire weather, (2) to investigate whether these trends are present in a variety of downscaled ESM data products, and (3) to explore the impact on future fire weather projections if the observed decline in relative humidity continues.

2 Results

2.1 Components of Historical Fire Weather Trends

The first question motivating the following results is: how has the observed drying trend in the Western United States contributed to historical trends in changing fire weather? To answer this, we calculate the Canadian Fire Weather Index (FWI) using historical reanalysis inputs from ERA5 and Daymet and estimate the isolated contribution from each of the four FWI input variables: temperature, relative humidity, precipitation, and wind speed. Figure 1a shows a clear upward trend in FWI over the 1980–2019 reanalysis period in the Western United States that may have contributed to the increase in wildfires reported by others (2).

Perhaps more surprising, however, is the relative contribution of each of the weather variables to this overall trend. As seen in Figure 1c, the largest contributor to the historical increases in FWI in the Western United States is the declining trends in relative humidity. Increasing temperatures do drive increases in FWI, as shown in Figure 1b, but the FWI trends are largely not statistically significant despite the temperature trends themselves being statistically significant (19). In many regions in the Western United States and especially the Southwest, the effect from declining relative humidity can be two to four times more powerful than the effect from increasing temperatures. Of course, changes in temperature also drive changes in relative humidity, but we see in Supplementary Figure 2 that 60-97% of the relative humidity trends and 67-84% of the FWI trends are caused by real changes in specific humidity, not changes in temperature driving down relative humidity.

The effect from changes in precipitation shown in Figure 1d are more spatially variable than the effect from temperature or relative humidity, but generally we see decreasing FWI from increasing precipitation in the North Great Plains and increasing FWI from declining precipitation in the Desert Southwest, although in the Desert Southwest this effect is still much smaller in magnitude than the effect from relative humidity. Last, in Figure 1e, we see the effect from changes in wind speed are smaller in magnitude than any of the other variables, although we can see a slightly positive increase in FWI from increasing wind speeds along a narrow vertical band in the Great Plains. Note there is substantial uncertainty in historical wind speed trends (20–22), and the results in Figure 1e are of lower confidence than the other variables.

Seasonal FWI trends based on reanalysis with individual variable contributions are shown in Supplementary Figure 3 through Supplementary Figure 6 and show similar relative contributions of the four independent variables to the overall FWI trend with minor differences depending on the region and season.

The FWI algorithm is a nonlinear function of the four independent variables, so we might expect the sum of individual FWI trend contributions from each variable would not be equivalent to the baseline calculation. However, Supplementary Figure 7 compares the baseline FWI trend to the

sum of the four individual variable trends and shows that in most regions in the contiguous United States, the sum of individual components is consistent in magnitude and spatial distribution to the baseline nonlinear calculation, giving us confidence that the decomposition in Figure 1 is meaningful. We do see some regions in Supplementary Figure 7 (e.g., the Cascade and Sierra mountain ranges) where the sum of contributions results in a much smaller FWI trend than the baseline calculation, indicating compounding factors are dominant here and the overall trend in FWI cannot be explained by the drying trend alone.

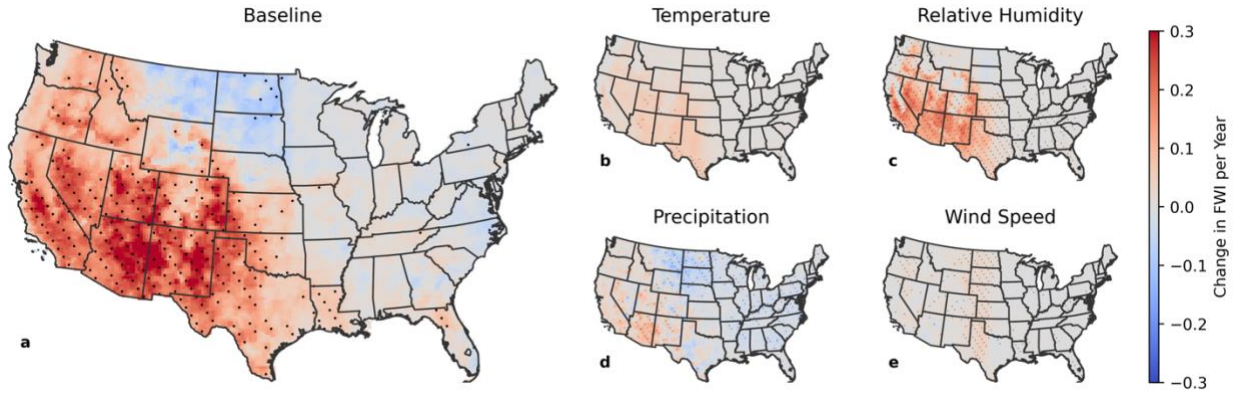

Figure 1. Historical trends of the annual Canadian Fire Weather Index (FWI) calculated from ERA5 and Daymet reanalysis data over the period 1980–2019. (a) Baseline historical FWI trend. (b) Historical trend based only on changes in near-surface air temperature. (c) Historical trend based only on changes in near-surface relative humidity. (d) Historical trend based only on changes in precipitation. (e) Historical trend based only on changes in near-surface wind speed. For panels (b–e), all variables other than the variable of interest are held constant at their 40-year historical mean value per pixel. Stippling indicates statistically significant trends ($p < 0.05$).

2.2 Humidity in Downscaled Earth System Model Data

Given the importance of declining relative humidity for historical changes in FWI illustrated in Figure 1 and the prevalence of fire weather projections derived from downscaled ESMs, we now ask to what extent different downscaling methods reproduce observed historical trends in relative humidity. The ESMs that are downscaled generally contradict observed humidity trends (10), and others have noted downscaling necessarily imports these errors (16). In Figure 2, we confirm this is true for four unique downscaling data products, with methods including generative machine learning, physics-based dynamical downscaling, and bias-correction-based statistical downscaling.

All four downscaled datasets assessed in Figure 2 generally reproduce trends found in the source ESM projections to varying degrees, with minor deviations depending on the method. In panels b and h of Figure 2, we can see the generative machine learning dataset Super-Resolution for Renewable Energy Resource Data with Climate Change Impacts (Sup3rCC) and the statistically downscaled dataset NASA Earth eXchange Global Daily Downscaled Projections (NASA-NEX-GDDP) strongly preserve their input trends with only minor deviation in magnitude and some elevation-dependence in Sup3rCC. This is expected given these are primarily statistical methods designed explicitly to preserve input trends. The physical downscaling methods, however, do not have these constraints.

The physical downscaling methods used in the Western United States Dynamically Downscaled Dataset (WUS-D3)and the Regional Climate Model version 4 (RegCM4) datasets shown in panels d and f of Figure 2 have greater deviations in both spatial patterning and trend magnitude but still preserve large-scale spatial trends from the source ESM. Interestingly, RegCM4 (and to a lesser extent WUS-D3) increases the relative humidity trend in the WUS when compared to the source ESM trend, which is in contradiction of the observations.

Seasonal patterns in relative humidity show similar results in Supplementary Figure 8 through Supplementary Figure 11 with ERA5 showing substantial drying trends in all four seasons. Some of the downscaled data and ESM pairs show substantial drying in the Western United States in certain seasons (for example in NASA-NEX-GDDP in the Fall; Supplementary Figure 11), but we see that this effect is only seasonal and averages out to minimal changes in Figure 2.

The spatial pattern of relative humidity trends varies substantially based on the individual realization of the source ESM, with each ESM showing varying levels of drying in the Western United States, although all at least an order of magnitude less than the observed trends. Although we only show one realization per downscaled dataset here, we focus on an ESM that was available in all downscaled data products with the best historical performance (23), and others have confirmed that the discrepancy of drying trends in the Western United States is a problem with virtually all ESMs from CMIP6 (10).

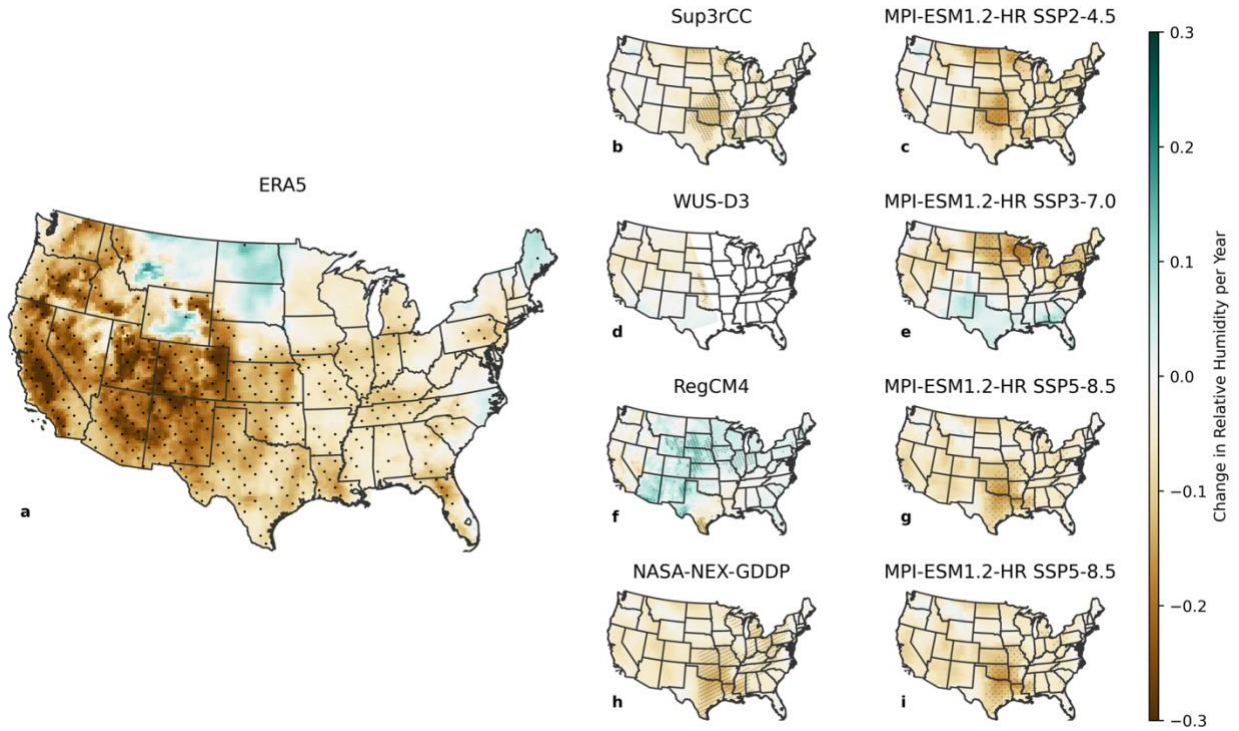

Figure 2. Trends in 1980–2019 annual near-surface relative humidity from (a) ERA5, (b, c) Sup3rCC and source ESM, (d, e) WUS-D3 and source ESM, (f, g) RegCM4 and source ESM, (h, i) NASA-NEX-GDDP and source ESM. Projections are based on the ESM MPI-ESM1.2-HR with the "historical" CMIP6 simulation through 2014 and after 2014: SSP2-4.5 r1i1p1f1 for (b, c), SSP3-7.0 r3i1p1f1 for (d, e), and SSP5-8.5 r1i1p1f1 for (f–i). The trend was calculated in (a–e) using daily minimum relative humidity, whereas in (f–i) using daily average relative humidity. Stippling indicates statistically significant trends ($p < 0.05$).

2.3 Humidity in Projections of Fire Weather

We now look to the impacts of the relative humidity trend discrepancy in long-term projections of the FWI. Considering the importance of historical declines in relative humidity for the FWI and the humidity bias in ESM projections, we can reasonably expect future projections will show substantially lower rates of increasing FWI compared to the observed historical trends. Indeed, in Figure 3, we can see the average 1980–2019 FWI trend calculated from the reanalysis data is frequently three to six times greater in the Western United States than the 2000–2039 trend calculated from the Sup3rCC five-member ensemble.

The FWI projections based on the Sup3rCC downscaled data shown in Figure 3b estimate a relatively spatially uniform increase in FWI across most of the contiguous United States based mostly on projected increases in air temperature. As shown in previous Sup3rCC documentation (24), there is less spatially coherent agreement on changes in relative humidity, precipitation, and wind speed, leading these variables to have a smaller contribution to average projected change in FWI.

To study future FWI projections under a continued drying scenario, we propose a simple method (detailed in Section 4.3) for enforcing the historical trend in relative humidity in our future projections of FWI by trend-correcting a downscaled relative humidity dataset. This is not a

perfect solution to the relative humidity problem, as it degrades the physical coherence of variables in the downscaled simulations, and we further discuss the motivation and limitations in Section 3. Nevertheless, we can see in Figure 3c that the trend-corrected projections substantially improve the FWI trends when compared to historical reanalysis trends.

Of course, the observed declines in relative humidity over the last four decades may be a temporary transient that could reverse back to a moistening trend, ultimately proving the ESM-based FWI projections to be skillful. However, if there are physical processes driving persistent humidity trends that are systematically misrepresented in the ESMs as proposed by (10), then ESM-based projections may prove to substantially underestimate future FWI trends.

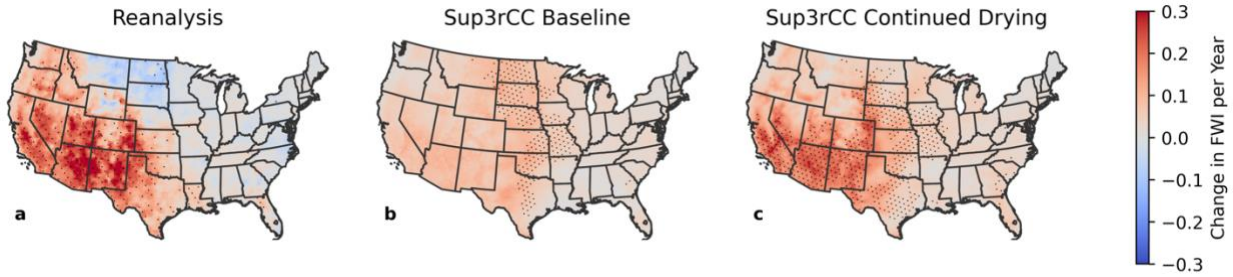

Figure 3. Trends in annual FWI based on (a) reanalysis data from ERA5 and Daymet over the time period 1980–2019, (b) Sup3rCC five-member ensemble over the time period 2000–2039, (c) continued drying scenario based on Sup3rCC five-member ensemble with trend-corrected relative humidity. Stippling indicates statistically significant trends ($p < 0.05$), and for panels (b) and (c), stippling also indicates three or more ensemble members agree on a statistically significant trend.

Figure 4 shows the results from the five-member Sup3rCC projections with and without the relative humidity trend correction using the metric of increase in number of days per year above the historical 95th percentile FWI (this threshold calculated per pixel from the 2000–2019 time period for each Sup3rCC member). We focus on increases here because, as shown in Supplementary Figure 12, there are almost no regions that show a projected decrease in extreme fire weather days.

Without the trend correction of relative humidity, we see little to no change in extreme fire weather days in the Western United States through the next two decades, including many regions without statistically significant changes in FWI distributions. With trend correction, we see many more extreme FWI days per year in the next two decades with notable hot spots in the California Central Valley and Northeast Colorado/Southwest Nebraska seeing more than 14 additional extreme fire weather days per year. We also see regions in Eastern Washington and Oregon, and in the Desert Southwest with 4-10 additional extreme days per year. Because our 95th percentile threshold sets 18 extreme fire weather days per location per year in the historical period, these regional increases represent a 20-70% increase in the rate of extreme days. Anecdotally, these trend-corrected projections appear to better match how wildfires have changed in the Western United States (especially extreme wildfires) since the 1980s (2).

We see how the projections vary in seasonal 95th percentile FWI in Supplementary Figure 13 through Supplementary Figure 17. We see that, in the winter, FWI conditions become more extreme in the Western United States with major impacts from the relative humidity trends (Supplementary Figure 14), whereas in the summer, FWI conditions become much more extreme in the Midwest with minor impact from relative humidity trends (Supplementary Figure 15). Fall months also see substantial increases throughout the Great Plains (Supplementary Figure 17), whereas spring months see the smallest changes of any season (Supplementary Figure 16).

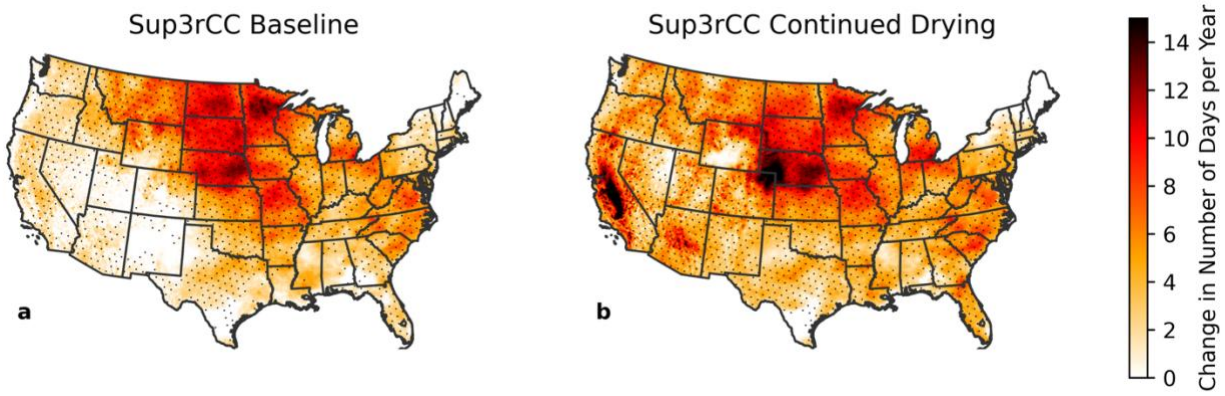

Figure 4. Increase in number of extreme fire weather days per year from 2000–2019 to 2020–2039 based on (a) Sup3rCC five-member ensemble and (b) continued drying scenario based on Sup3rCC five-member ensemble with trend-corrected relative humidity. Extreme fire weather days are defined as days with FWI above the 95th percentile value calculated per pixel over the 2000–2019 period. Stippling indicates where three or more ensemble members agree on an increase in extreme FWI days and a statistically significant shift in 20-year distributions ($p < 0.05$).

3 Discussion and Conclusion

In this work, relative humidity emerges as the dominant driver of both historical and projected trends in fire weather across the Western United States. While temperature and precipitation contribute to fire weather variability, declines in relative humidity in many regions exert an effect several times larger as measured by the Canadian FWI. This result implies that drying in the actual atmospheric water vapor content (specific humidity) is a key mechanism underlying the observed increase in fire weather risk and that the divergence between observations and ESM simulations reported by (10) is crucial for understanding changes in fire weather. (10) suggests that observed aridification may arise from lower land-surface moisture availability or more efficient drying processes than represented in many ESMs. Under warming, evapotranspiration initially increases, but once surface moisture becomes limiting, specific humidity cannot continue to rise and atmospheric drying results. Additional model biases such as excessive evaporation, errors in moisture transport, or unrealistic coupling between atmospheric moisture and precipitation may further contribute to discrepancies between simulated and observed moisture trends. These structural differences suggest that near-term projections derived from ESMs may inherit biases in atmospheric moisture dynamics, particularly in specific and relative humidity, with implications for interpreting projected changes in fire weather risk.

ESMs are frequently downscaled to more regional climates before being used to estimate fire weather risk, however, we find four unique methods of downscaling ESM projections all carry forward this discrepancy in humidity trends. As such, fire weather metrics derived from downscaled ESM data products are highly likely to underestimate the upward trend of fire weather in the Western United States over the historical time period. There are several such downscaled data products currently in use for real-world decision-making on future fire risk (25–28). We cannot reliably assess the skill of these downscaled data products for the future time period without future observations, yet based on the inaccurate representation of declining relative humidity over the historical period, caution may be warranted in using these projections as a foundation for real-world fire weather resilience decision-making. The drying trends observed in the Western United States since approximately the 1980s could prove to be temporary; however, if the physical processes related to humidity are systematically misrepresented in ESMs, as suggested by (10), then these downscaled ESM-based projections are likely to substantially underestimate future FWI trends.

To study a continued drying fire weather scenario, we propose trend-correcting the relative humidity variable in downscaled projections. This assumes the observed declines in relative humidity in the Western United States will continue into the future (time stationarity). This approach is not intended as a physics-based or final solution to the humidity biases in ESMs, but rather as an interim method for assessing the sensitivity of future FWI projections to the observed historical drying trend. The trend correction corrupts the physical coherence between variables, and physics-informed simulations would manifest the impacts of this change on other related variables. Nevertheless, this approach has merit in its contribution of a hypothetical continued drying scenario, which may be useful in the near-term before we fully understand the role of humidity trends in the Earth system. The motivation for considering trend-corrected humidity projections is that ESMs contradict observations crucial to the quantification of changing fire weather, which could lead us to inadequately prepare today for the fire weather of tomorrow. Planning for future changes in fire weather based on current ESM data (Figure 3b) largely ignores substantial historical changes (Figure 3a). Ultimately, fire weather projections with trend-corrected humidity may not prove to be skillful representation of future changes, but we hope these projections will serve as a useful quantification of the importance and uncertainty in humidity trends, spurring conversation and improvement in our understanding of changing fire weather regimes.

4 Materials and Methods

4.1 Fire Weather Index

Throughout this work, we use the FWI as a metric for quantifying the overall fire risk from weather factors (29). The FWI uses daily atmospheric weather variable inputs to estimate the risk of fire ignition and spread. Notably, the metric does not include vegetation or fuel availability (although it does indirectly model fuel moisture content), sources of ignition, or fire suppression. We use the FWI here instead of other similar fire weather metrics because of its ubiquity in similar studies (14, 15, 18). There are a number of similar commonly used fire weather metrics, but they consist primarily of similar combinations of the same weather variables, and the Canadian FWI has previously been recommended as the most skillful (30).

The FWI takes in daily metrics from four weather variables. For our calculations, we use daily maximum temperature, daily minimum relative humidity, daily average wind speed, and daily total precipitation. We use these daily extrema in temperature and humidity as they drive more extreme fire weather conditions than daily averages alone.

To study the isolated contribution of each of the four weather input variables to the overall FWI trends, we run four calculations based on historical reanalysis data, where three of the four input variables are held constant at their 1980–2019 mean value (per pixel), whereas the fourth variable is the original time series data. This effectively calculates the partial derivative of the FWI with respect to the historical trends of each input variable. This is in addition to the normal FWI calculation based on the original reanalysis input data with no variables held constant.

4.2 Data Sources

For historical analysis, we use ERA5 reanalysis data (31) for temperature, humidity, and wind speeds combined with Daymet v4 data (32) for precipitation. ERA5 is used at its native 31-km resolution, and Daymet v4 is aggregated from its native 4-km resolution to the ERA5 grid.

We use gridded reanalysis data for historical weather, relying on previous validation showing that ERA5 performs adequately for historical extreme heat events (33, 34) and humidity trends (9, 10) and that Daymet performs adequately for historical precipitation (32). Wind data is more challenging, and we acknowledge the spatial resolution of ERA5 is unlikely to properly resolve extreme wind events (35) that can drive extreme wildfire conditions. Given the active debate and associated uncertainty in historical trends and changing wind regimes (20–22), we accept the ERA5 wind data as adequate for this study given wind's relatively small contribution to overall trends.

For future projections, we evaluate a number of downscaling methods and source ESM datasets. We aim to represent a wide range of downscaled data products each with unique methods that are commonly used throughout the literature. Downscaled datasets represent substantial effort, compute costs, and storage volumes. Accordingly, not all downscaled datasets have the same ESMs, shared socioeconomic pathways (SSPs), or simulation variants. In the near-future through 2040, the uncertainty from different SSPs is typically smaller than that from natural variability or model formulation (36, 37), so here we focus on comparisons across downscaling products with the same ESM.

For a machine learning downscaled product, we evaluate the Sup3rCC v0.2.2 dataset. This downscaling product uses generative adversarial networks, a form of generative machine learning, to downscale 100-km daily ESM data to 4-km hourly data (24, 38). We use five members of the Sup3rCC dataset, each from the SSP2-4.5.

For physics-based dynamically downscaled data, we use the WUS-D3 (39) and data produced with the RegCM4 (40). The WUS-D3 dataset is downscaled using the Weather Research and Forecast model based on the SSP3-7.0 and is available at a 9-km hourly resolution over the Western United States. (all other datasets are available over all of the contiguous United States). The RegCM4 data was produced for SSP5-8.5 at a 25-km resolution before daily outputs were bias corrected to 4 km using Daymet v4.

For a purely statistical downscaling method, we use the NASA-NEX-GDDP version 1.0 (41). This dataset was downscaled using the bias-correction with spatial disaggregation method to approximately a 25-km resolution based on CMIP6 data. Although multiple SSPs are available for NASA-NEX-GDDP, we only use the SSP5-8.5 scenario, which compares directly against the RegCM4 dataset.

Another widely used family of statistical downscaling methods is based on the constructed analog approach. Although constructed analog downscaling approaches are not considered here, there have been previous studies demonstrating fire risk derived from downscaled data using these methods understates historical fire weather trends while highlighting relative humidity model biases as a driving factor (18).

For the four downscaled CMIP6 projection datasets, we compare relative humidity trends for a single downscaled ESM based on the higher-resolution version of the Max Planck Institute Earth System Model (MPI-ESM1.2-HR) (42) alongside the source ESM trends without downscaling. For the relative humidity trends, we use only a single ESM realization for comparison to illustrate the trends in the source ESM simulation and to directly show how each downscaling method handles these trends. We select MPI-ESM1.2-HR as the best performing ESM that was available in all downscaled data products based on a rigorous evaluation of CMIP6 ESMs over the contiguous United States (23).

We are limited by data availability in the downscaled data products, so we compare different SSPs and variants across the four downscaling products: SSP2-4.5 r1i1p1f1 for Sup3rCC, SSP3-7.0 r3i1p1f1 for WUS-D3, SSP5-8.5 r1i1p1f1 for RegCM4, and SSP5-8.5 r1i1p1f1 for NASA-NEX-GDDP. All data products use the "historical" CMIP6 simulation through the year 2014 with the noted SSP simulations starting in 2015. Additionally, we focus on daily minimum relative humidity for the hourly downscaled datasets Sup3rCC and WUS-D3, as daily minimum relative humidity typically corresponds with the greatest fire weather risk. Unfortunately, RegCM4 and NASA-NEX-GDDP only contain daily average relative humidity, so we only present the trends in daily average values for these datasets. Despite the heterogeneity of ESM realizations and daily minimum versus average relative humidity, we see comparable results across all ESMs and downscaled data products.

A summary of all the data sources used in this work, the variables used, and what they were used to calculate is presented in Table 1.

Table 1. Data sources used in this work.

Name	Temporal Extent Used	Variables Used	Used to Calculate	Notes
ERA5	1980-2019	Near-surface daily maximum temperature, daily minimum relative humidity, daily average windspeed	FWI trends, relative humidity trends, relative humidity trend corrections for Sup3rCC	(31)
Daymet	1980-2019	Daily total precipitation	FWI trends	(32)

Sup3rCC	1980-2039	Near-surface daily maximum temperature, daily minimum relative humidity, daily average windspeed, daily total precipitation	FWI trends, relative humidity trends, projected changes in FWI extreme days and FWI statistics	Used five ensemble members based on EC-Earth3-CC, EC-Earth3-Veg, GFDL-CM4, MPI-ESM-1.2-HR, and TaiESM1 all from SSP2-4.5 r1i1p1f1 (24, 38)
WUS-D3	1980-2019	Daily minimum near-surface relative humidity	Relative humidity trends	Based on MPI-ESM-1.2-HR SSP3-7.0 r3i1p1f1 (39)
RegCM4	1980-2019	Daily average Near-surface relative humidity	Relative humidity trends	Based on MPI-ESM-1.2-HR SSP5-8.5 r1i1p1f1 (40)
NASA-NEX-GDDP	1980-2019	Daily average Near-surface relative humidity	Relative humidity trends	Based on MPI-ESM-1.2-HR SSP5-8.5 r1i1p1f1 (41)
MPI-ESM-1.2-HR	1980-2019	Daily average and daily minimum Near-surface relative humidity	Relative humidity trends	SSPs and variants corresponding to the downscaled data products (42)

4.3 Trends in Humidity and the Canadian Fire Weather Index

For the calculation of trends in relative humidity and FWI, we fit a linear regression to the daily average time series per pixel over the period of interest and then report the slope of that line in units of change per year (change in relative humidity or FWI). For example, when calculating the annual trend in FWI for ERA5 over 1980–2019, we fit a linear regression $y = mx + b$ where y is the 14,610 daily FWI values (365 days for 40 years plus 10 leap days), $x \in \mathbb{R}$ is the evenly-spaced time index in the range [0, 40) for the 40 years, b is a y-intercept (not reported), and m is the reported trend in units of change in FWI per year. For seasonal trends, we apply a mask to the daily data before fitting the linear regression such that we are fitting only the days belonging to each respective season. We implemented daily data trends for simplicity instead of fitting monthly or annual mean values and found minimal differences when spot checking daily versus monthly trends.

We report measures of statistical significance for relative humidity and FWI trends and distribution shifts. For 40-year daily trends in Section 2.1 and 2.2, statistical significance was assessed at each pixel using heteroskedasticity- and autocorrelation-consistent standard errors (43) with significance evaluated at the 5% level ($p < 0.05$). The statistical significance of daily trends is evaluated only for the entire 40-year daily time series and not for unevenly spaced seasonal time series.

For distribution shifts and changes in extreme FWI metrics in Section 2.3, we use the Kolmogorov-Smirnov test (44) at each pixel to compare daily FWI distributions from the 2000–2019 time period to the 2020–2039 time period with significance evaluated again at the 5% level ($p < 0.05$). The statistical significance of distribution shifts from 2000–2019 to 2020–2039 is evaluated using the distributions of multiyear annual daily FWI values from the 20-year periods

as well as the distributions of daily values from only the respective multiyear seasonal daily value distributions.

To study how projections of FWI might differ if the observed drying trends continue, we study projections with the historical 40-year drying trend superimposed on the ESM-based projections. To do this, we calculate the 40-year linear fits for ERA5 and the source ESMs used in Sup3rCC, both over the time period 1980–2019. We linearly interpolate the fit parameters across space onto the Sup3rCC grid such that they can be compared against each other (ERA5 versus ESM) at every higher-resolution Sup3rCC pixel. We vertically y-shift the ESM trend so that it intercepts the ERA5 trend on January 1, 2010, such that there is no correction performed in the middle of our "historical" period, which we define as 2000–2019. Finally, at every pixel and every timestep in the Sup3rCC data, we calculate a correction factor as the ratio of the ERA5 linear regression divided by the ESM linear regression and multiply the Sup3rCC relative humidity by this value. This procedure is described by Equation 1:

$$\widehat{RH} = RH \frac{M_{ERA5}x + B_{ERA5}}{M_{ESM}x + B_{ESM} + \Delta_{ESM}} \quad \text{Equation 1}$$

where $\widehat{RH}$ is the trend-corrected relative humidity based on the original downscaled relative humidity RH, M_{ERA5} and B_{ERA5} are the slope and y-intercept of the linear regression of the ERA5 relative humidity data, M_{ESM} and B_{ESM} are the slope and y-intercept of the linear regression of the ESM relative humidity data, $x \in \mathbb{R}$ is a real-valued time index for the Sup3rCC temporal extent, and Δ_{ESM} is a y-shift factor that makes the ESM trend line intercept the ERA5 trend line in 2010. $\widehat{RH}$ values greater than 100 are prevented in the calculation of the FWI. This procedure is illustrated for a single location in Supplementary Figure 1.

5 Data Availability

This work is based entirely on the publicly available data sources listed in Table 1. Distilled results will be publicly released via the Open Energy Data Initiative upon acceptance of this manuscript.

6 Acknowledgments

We thank Jaemo Yang, Meghan Mooney, Mark Ruth, Ryan Burg, and Elizabeth Doris for their thoughtful reviews of the initial draft and Jennifer Korte for her invaluable help editing the manuscript.

This work was authored by the National Laboratory of the Rockies for the U.S. Department of Energy (DOE) operated under Contract No. DE-AC36-08GO28308, by Oak Ridge National Laboratory operated under Contract No. DE-AC05-00OR22725, and by the University of Wyoming. This research was supported by the Grid Modernization Initiative of the U.S. Department of Energy (DOE) as part of its Grid Modernization Laboratory Consortium, a strategic partnership between DOE and the national laboratories to bring together leading experts, technologies, and resources to collaborate on the goal of modernizing the nation's grid. Funding provided by the DOE Office of Energy Efficiency and Renewable Energy (EERE), the

DOE Office of Electricity (OE), and the DOE Office of Cybersecurity, Energy Security, and Emergency Response (CESER). Drs. Liu and Rahimi were supported under the National Science Foundations' (NSF's) EPSCoR Grant OIA-2149105: Wyoming Anticipating the Climate-Water Transition and the NSF CO-WY ASCEND, grant NSF-2315760. This research was performed using computational resources sponsored by the U.S. Department of Energy's Office of Critical Minerals and Energy Innovation and located at the National Laboratory of the Rockies. We would also like to acknowledge Computational and Information Systems Laboratory (CISL) in support of the NSF NCAR-Wyoming Supercomputing Center (NWSC). The views expressed in the article do not necessarily represent the views of the DOE or the U.S. Government. The U.S. Government retains and the publisher, by accepting the article for publication, acknowledges that the U.S. Government retains a nonexclusive, paid-up, irrevocable, worldwide license to publish or reproduce the published form of this work, or allow others to do so, for U.S. Government purposes.

7 References

1. A. R. Carlson, *et al.*, Rising rates of wildfire building destruction in the conterminous United States. *Proceedings of the National Academy of Sciences* **122**, e2505886122 (2025).

2. V. Iglesias, J. K. Balch, W. R. Travis, U.S. fires became larger, more frequent, and more widespread in the 2000s. *Science Advances* **8**, eabc0020 (2022).

3. D. Thomas, D. Butry, S. Gilbert, D. Webb, J. Fung, "The costs and losses of wildfires: a literature survey" (National Institute of Standards and Technology, 2017).

4. U.S. Congress, "Climate-exacerbated wildfires cost the U.S. between $394 to $893 billion each year in economic costs and damages" (U.S. Congress Joint Economic Committee, 2023).

5. J. I. Levine, B. M. Collins, Z. L. Steel, P. de Valpine, S. L. Stephens, Higher incidence of high-severity fire in and near industrially managed forests. *Frontiers in Ecology and the Environment* **20**, 397–404 (2022).

6. E. J. Fusco, J. T. Finn, J. K. Balch, R. C. Nagy, B. A. Bradley, Invasive grasses increase fire occurrence and frequency across US ecoregions. *Proceedings of the National Academy of Sciences* **116**, 23594–23599 (2019).

7. V. Iglesias, *et al.*, Risky Development: Increasing Exposure to Natural Hazards in the United States. *Earth's Future* **9**, e2020EF001795 (2021).

8. J. T. Abatzoglou, A. P. Williams, Impact of anthropogenic climate change on wildfire across western US forests. *Proceedings of the National Academy of Sciences* **113**, 11770–11775 (2016).

9. T. W. P. Jacobson, *et al.*, An Unexpected Decline in Spring Atmospheric Humidity in the Interior Southwestern United States and Implications for Forest Fires. (2024). https://doi.org/10.1175/JHM-D-23-0121.1.

10. I. R. Simpson, *et al.*, Observed humidity trends in dry regions contradict climate models. *Proceedings of the National Academy of Sciences* **121**, e2302480120 (2024).

11. M. P. Byrne, P. A. O'Gorman, Trends in continental temperature and humidity directly linked to ocean warming. *Proceedings of the National Academy of Sciences* **115**, 4863–4868 (2018).

12. Y. Kim, M. S. Johnson, Deciphering the role of evapotranspiration in declining relative humidity trends over land. *Commun Earth Environ* **6**, 105 (2025).

13. Y. He, Z. Zhou, E.-S. Im, H.-H. Kwon, Wildfire risk in a changing climate: Evaluating fire weather indices and their global patterns with CMIP6 multi-model projections. *Weather and Climate Extremes* **48**, 100751 (2025).

14. C. Gallo, *et al.*, Future Impacts of Climate Change on Global Fire Weather: Insight from Weighted CMIP6 Multimodel Ensembles. *Journal of Climate* (2025). https://doi.org/10.1175/JCLI-D-24-0540.1.

15. S. Feng, J. Zscheischler, Z. Hao, E. Bevacqua, Growing human-induced climate change fingerprint in regional weekly fire extremes. *npj Clim Atmos Sci* **8**, 152 (2025).

16. H. Clarke, *et al.*, Gazing into the flames: A guide to assessing the impacts of climate change on landscape fire. *Science Advances* **11**, eadz2429 (2025).

17. United Nations Environment Programme, GRID-Arendal, Spreading like Wildfire: The Rising Threat of Extraordinary Landscape Fires - A Rapid Response Assessment. (2022). https://wedocs.unep.org/handle/20.500.11822/38372.

18. T. C. Avila, *et al.*, Downscaled CMIP5 projections of physical fire risk understate historical trends. *Environ. Res. Lett.* **20**, 084025 (2025).

19. R. S. Vose, S. Applequist, M. J. Menne, C. N. Williams, P. Thorne, An intercomparison of temperature trends in the U.S. Historical Climatology Network and recent atmospheric reanalyses. *Geophysical Research Letters* **39**, 2012GL051387 (2012).

20. S. C. Pryor, *et al.*, Wind speed trends over the contiguous United States. *Journal of Geophysical Research: Atmospheres* **114** (2009).

21. Z. Zeng, *et al.*, A reversal in global terrestrial stilling and its implications for wind energy production. *Nat. Clim. Chang.* **9**, 979–985 (2019).

22. G. A. Meehl, *et al.*, Earth, wind and fire: Are Boulder's extreme downslope winds changing? (2025). https://doi.org/10.1175/BAMS-D-24-0091.1.

23. M. Ashfaq, D. Rastogi, M. A. Abid, S.-C. Kao, Evaluation of CMIP6 GCMs over the CONUS for downscaling studies. [Preprint] (2022). Available at: http://www.essoar.org/doi/10.1002/essoar.10510589.1 [Accessed 23 September 2022].

24. G. Buster, *et al.*, Second-generation downscaled earth system model data using generative machine learning. *Data in Brief* **61** (2025).

25. A. L. Westerling, Wildfire Simulations for California's Fourth Climate Change Assessment: Projecting Changes in Extreme Wildfire events with a Warming Climate. (2018). https://doi.org/CCCA4-CEC-2018-014.

26. E. K. Brown, J. Wang, Y. Feng, US wildfire potential: a historical view and future projection using high-resolution climate data. *Environ. Res. Lett.* **16**, 034060 (2021).

27. K. Riley, *et al.*, Spatial datasets of probabilistic wildfire risk components for the conterminous United States (270m) for circa 2011 climate and projected future climate circa 2047. https://doi.org/10.2737/RDS-2025-0006. Deposited 1 July 2025.

28. J. Sury, S. E. Hansen, Q. Krasniqi, A. Samur, J. Schlegelmilch, U.S. Natural Hazards Climate Change Projections. (2025). https://doi.org/10.7916/e93y-fm30.

29. C. E. Van Wagner, T. L. Pickett, *Equations and FORTRAN program for the Canadian forest fire weather index system* (1985).

30. J. Castel-Clavera, *et al.*, A comparative analysis of fire-weather indices for enhanced fire activity prediction with probabilistic approaches. *Agricultural and Forest Meteorology* **361**, 110315 (2025).

31. H. Hersbach, *et al.*, "ERA5 hourly data on single levels from 1940 to present" (Copernicus Climate Change Service (C3S) Climate Data Store (CDS), 2018).

32. P. E. Thornton, *et al.*, Gridded daily weather data for North America with comprehensive uncertainty quantification. *Sci Data* **8**, 190 (2021).

33. S. C. Sheridan, C. C. Lee, E. T. Smith, A Comparison Between Station Observations and Reanalysis Data in the Identification of Extreme Temperature Events. *Geophysical Research Letters* **47**, e2020GL088120 (2020).

34. E. Smith, N. Grant, X. Luo, D. Diaz, Evaluating the ability of gridded climate datasets to capture temperature and precipitation trends and extremes. *Sci Rep* **15**, 12607 (2025).

35. S. Jafari, T. Sommer, N. Chokani, R. S. Abhari, Wind Resource Assessment Using a Mesoscale Model: The Effect of Horizontal Resolution in (American Society of Mechanical Engineers Digital Collection, 2013), pp. 987–995.

36. A. Wootten, A. Terando, B. J. Reich, R. P. Boyles, F. Semazzi, Characterizing Sources of Uncertainty from Global Climate Models and Downscaling Techniques. *Journal of Applied Meteorology and Climatology* **56**, 3245–3262 (2017).

37. E. Hawkins, R. Sutton, The Potential to Narrow Uncertainty in Regional Climate Predictions. *Bulletin of the American Meteorological Society* **90**, 1095–1108 (2009).

38. G. Buster, B. N. Benton, A. Glaws, R. N. King, High-resolution meteorology with climate change impacts from global climate model data using generative machine learning. *Nat Energy* 1–13 (2024). https://doi.org/10.1038/s41560-024-01507-9.

39. S. Rahimi, *et al.*, An overview of the Western United States Dynamically Downscaled Dataset (WUS-D3). *Geoscientific Model Development* **17**, 2265–2286 (2024).

40. S.-C. Kao, *et al.*, "The Third Assessment of the Effects of Climate Change on Federal Hydropower" (Oak Ridge National Lab. (ORNL), Oak Ridge, TN (United States), 2022).

41. NASA Earth Exchange (NEX) Global Daily Downscaled Projections (GDDP) dataset. https://registry.opendata.aws/nex-gddp-cmip6/. https://doi.org/10.7917/OFSG3345.

42. W. A. Müller, *et al.*, A Higher-resolution Version of the Max Planck Institute Earth System Model (MPI-ESM1.2-HR). *Journal of Advances in Modeling Earth Systems* **10**, 1383–1413 (2018).

43. W. K. Newey, K. D. West, A Simple, Positive Semi-Definite, Heteroskedasticity and Autocorrelation Consistent Covariance Matrix. *Econometrica* **55**, 703–708 (1987).

44. I. M. Chakravarti, R. G. Laha, Roy, *Handbook of Methods of Applied Statistics, Volume I*.

Supplementary Information

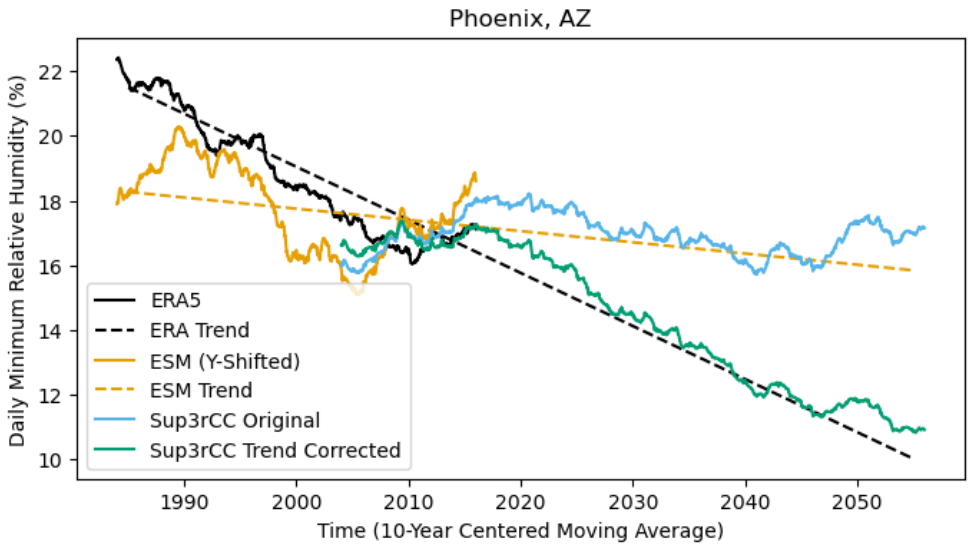

Supplementary Figure 1. Illustration of the relative humidity trend correction procedure.

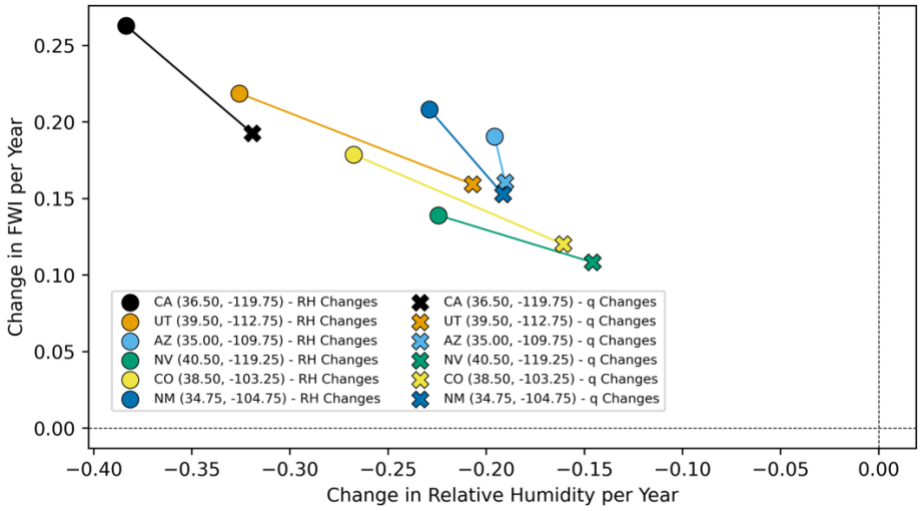

Supplementary Figure 2. Historical trends in daily minimum relative humidity (RH) versus trends in RH from only changes in specific humidity (q) (i.e., no changes in RH due to change in temperature) and the resulting trends in FWI. Data is taken at single reanalysis pixels from 1980-2019 in six states in the Southwest that have large positive historical FWI trends. Similar to Figure 1c, the FWI trends are calculated with fixed average temperature, wind speed, and precipitation inputs to isolate the effects of changing humidity on the FWI.

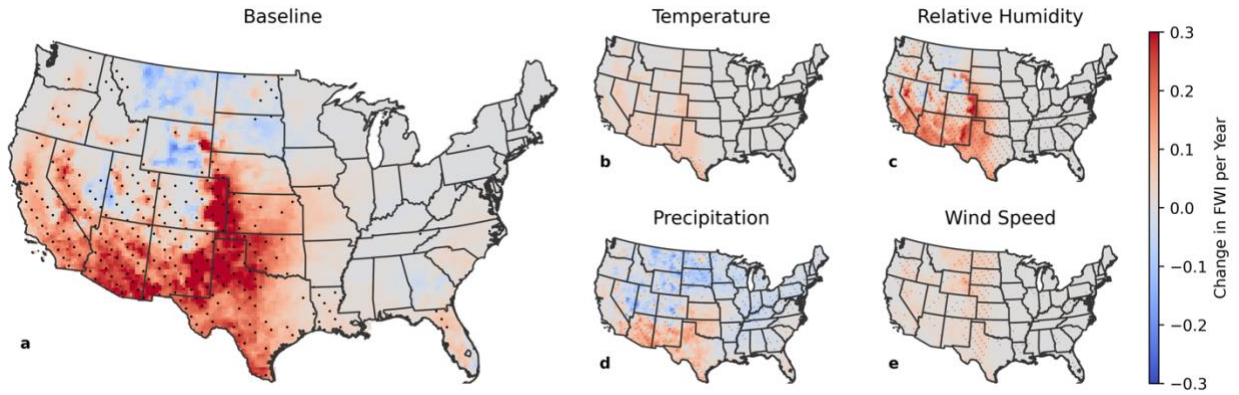

Supplementary Figure 3. Historical trends of the winter (December, January, February) Canadian Fire Weather Index (FWI) calculated from ERA5 and Daymet reanalysis data over the period 1980–2019. (a) Baseline historical FWI trend. (b) Historical trend based only on changes in near-surface air temperature. (c) Historical trend based only on changes in near-surface relative humidity. (d) Historical trend based only on changes in precipitation. (e) Historical trend based only on changes in near-surface wind speed. For panels (b–e), all variables other than the variable of interest are held constant at their 40-year historical mean value per pixel. Stippling indicates statistically significant trends ($p < 0.05$).

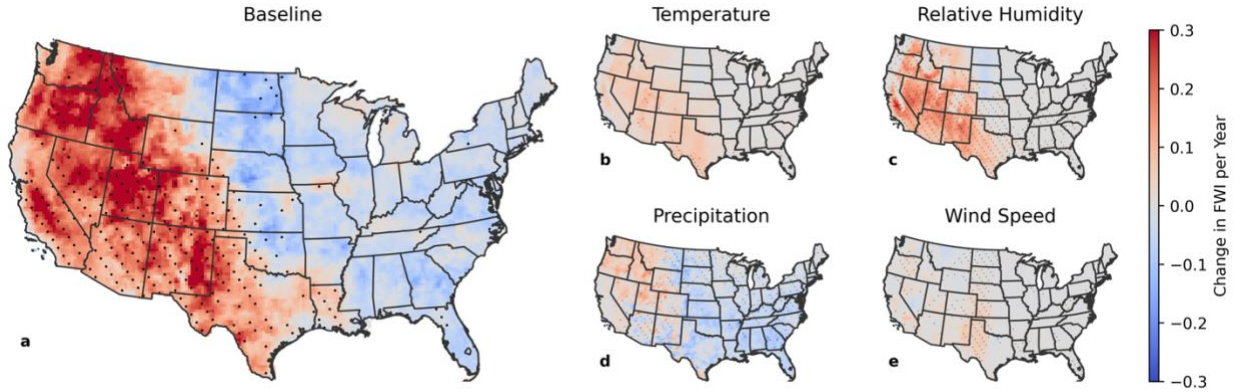

Supplementary Figure 4. Historical trends of the summer (June, July, August) Canadian FWI calculated from ERA5 and Daymet reanalysis data over the period 1980–2019. (a) Baseline historical FWI trend. (b) Historical trend based only on changes in near-surface air temperature. (c) Historical trend based only on changes in near-surface relative humidity. (d) Historical trend based only on changes in precipitation. (e) Historical trend based only on changes in near-surface wind speed. For panels (b–e), all variables other than the variable of interest are held constant at their 40-year historical mean value per pixel. Stippling indicates statistically significant trends ($p < 0.05$).

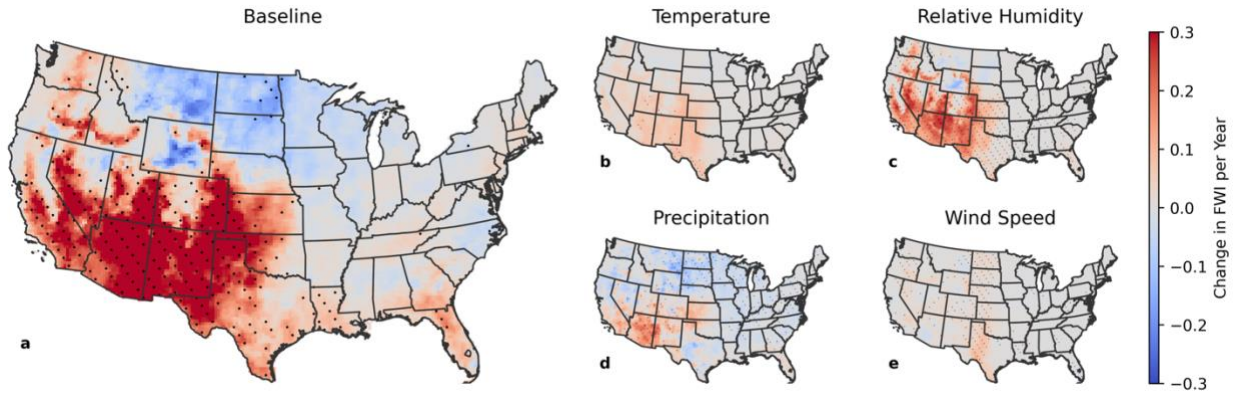

Supplementary Figure 5. Historical trends of the spring (March, April, May) Canadian FWI calculated from ERA5 and Daymet reanalysis data over the period 1980–2019. (a) Baseline historical FWI trend. (b) Historical trend based only on changes in near-surface air temperature. (c) Historical trend based only on changes in near-surface relative humidity. (d) Historical trend based only on changes in precipitation. (e) Historical trend based only on changes in near-surface wind speed. For panels (b–e), all variables other than the variable of interest are held constant at their 40-year historical mean value per pixel. Stippling indicates statistically significant trends ($p < 0.05$).

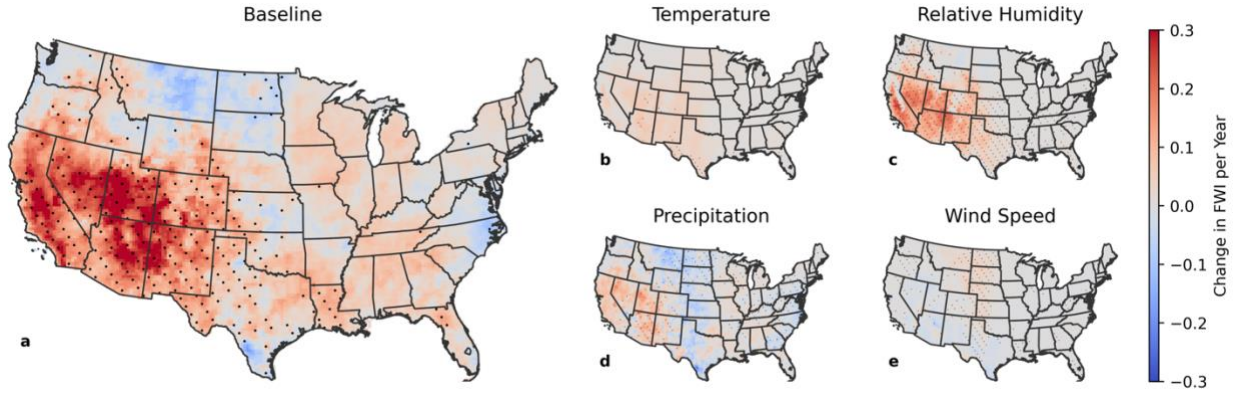

Supplementary Figure 6. Historical trends of the fall (September, October, November) Canadian FWI calculated from ERA5 and Daymet reanalysis data over the period 1980–2019. (a) Baseline historical FWI trend. (b) Historical trend based only on changes in near-surface air temperature. (c) Historical trend based only on changes in near-surface relative humidity. (d) Historical trend based only on changes in precipitation. (e) Historical trend based only on changes in near-surface wind speed. For panels (b–e), all variables other than the variable of interest are held constant at their 40-year historical mean value per pixel. Stippling indicates statistically significant trends ($p < 0.05$).

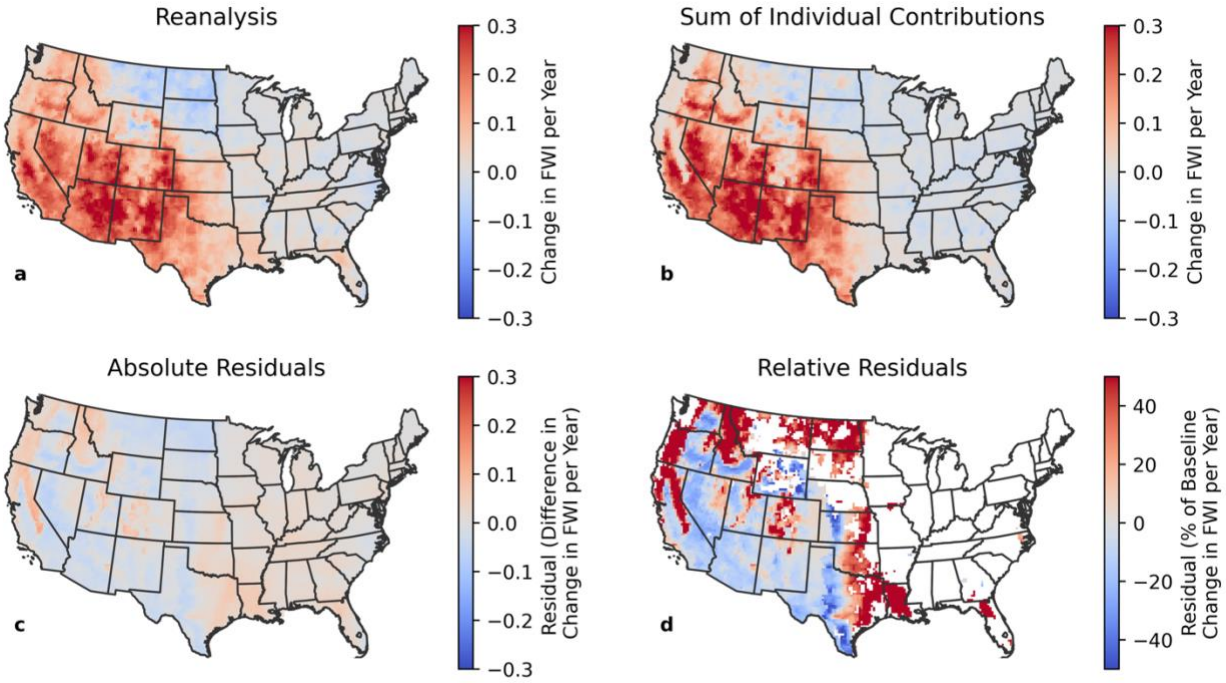

Supplementary Figure 7. Comparison of baseline historical trends of the annual Canadian FWI (a) against the sum of individual variable contributions (b) from temperature, relative humidity, precipitation, and wind speed. Panels (c) and (d) show the residual (i.e., difference in trend) between the baseline FWI calculation and the sum of individual contributions in absolute and relative units, respectively. For relative residuals (d), pixels with absolute baseline trends less than 0.05 per year are not shown to avoid divide by zero operations and appear as white.

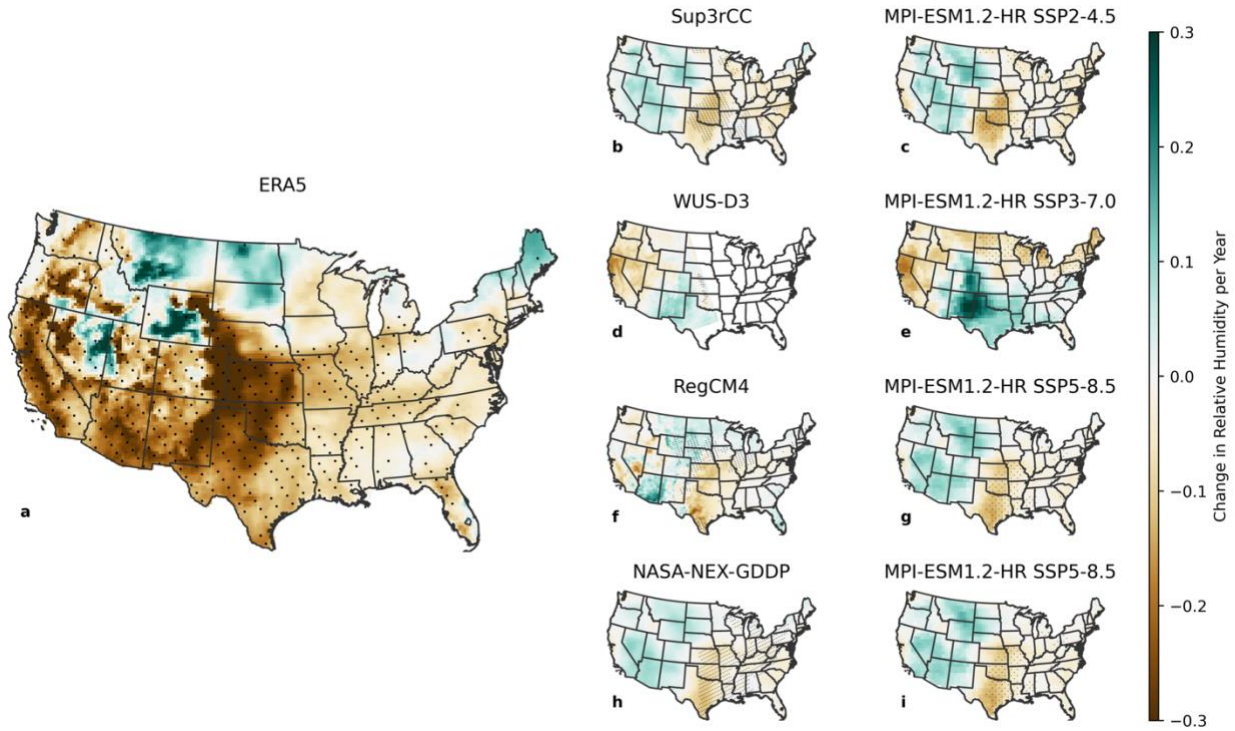

Supplementary Figure 8. Trends in 1980–2019 winter (December, January, February) near-surface relative humidity from (a) ERA5, (b, c) Sup3rCC and source ESM, (d, e) WUS-D3 and source ESM, (f, g) RegCM4 and source ESM, (h, i) NASA-NEX-GDDP and source ESM. Projections are based on the ESM MPI-ESM1.2-HR with the "historical" CMIP6 simulation through 2014 and after 2014: SSP2-4.5 r1i1p1f1 for (b, c), SSP3-7.0 r3i1p1f1 for (d, e), and SSP5-8.5 r1i1p1f1 for (f–i). The trend was calculated in (a–e) using daily minimum relative humidity, whereas in (f–i) using daily average relative humidity. Stippling indicates statistically significant trends ($p < 0.05$).

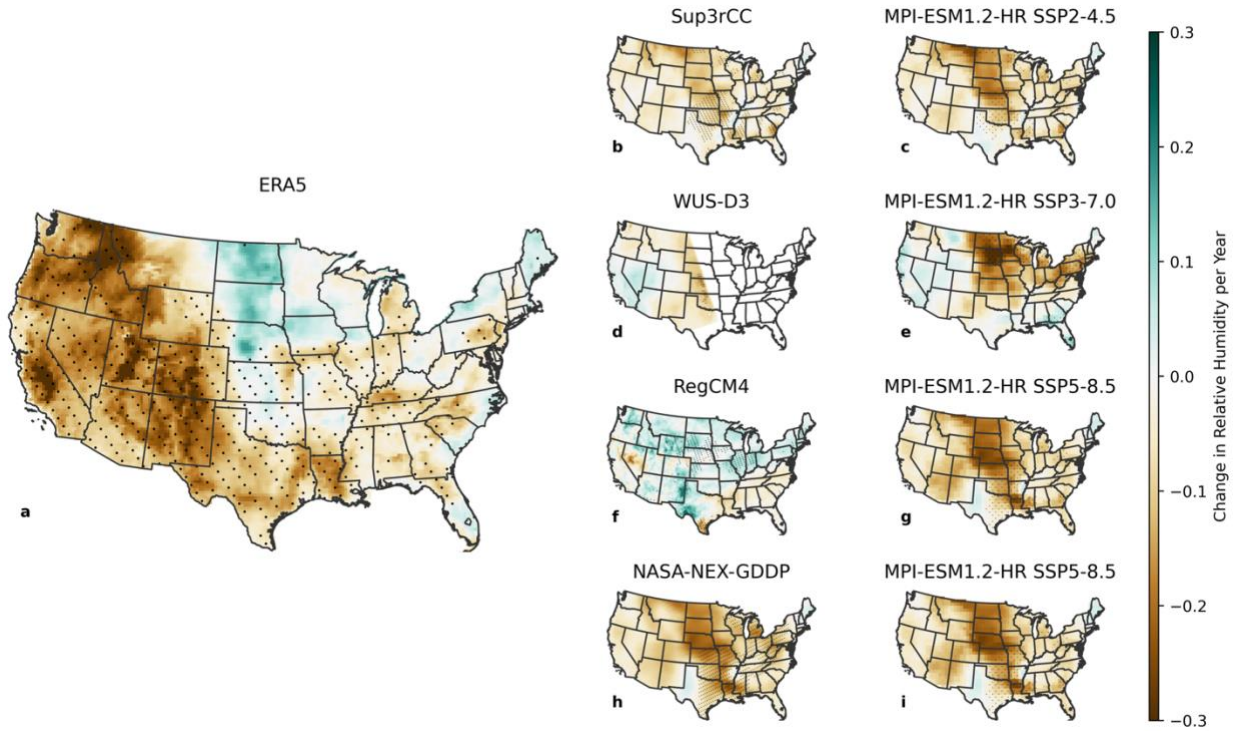

Supplementary Figure 9. Trends in 1980–2019 summer (June, July, August) near-surface relative humidity from (a) ERA5, (b, c) Sup3rCC and source ESM, (d, e) WUS-D3 and source ESM, (f, g) RegCM4 and source ESM, (h, i) NASA-NEX-GDDP and source ESM. Projections are based on the ESM MPI-ESM1.2-HR with the "historical" CMIP6 simulation through 2014 and after 2014: SSP2-4.5 r1i1p1f1 for (b, c), SSP3-7.0 r3i1p1f1 for (d, e), and SSP5-8.5 r1i1p1f1 for (f–i). The trend was calculated in (a–e) using daily minimum relative humidity, whereas in (f–i) using daily average relative humidity. Stippling indicates statistically significant trends ($p < 0.05$).

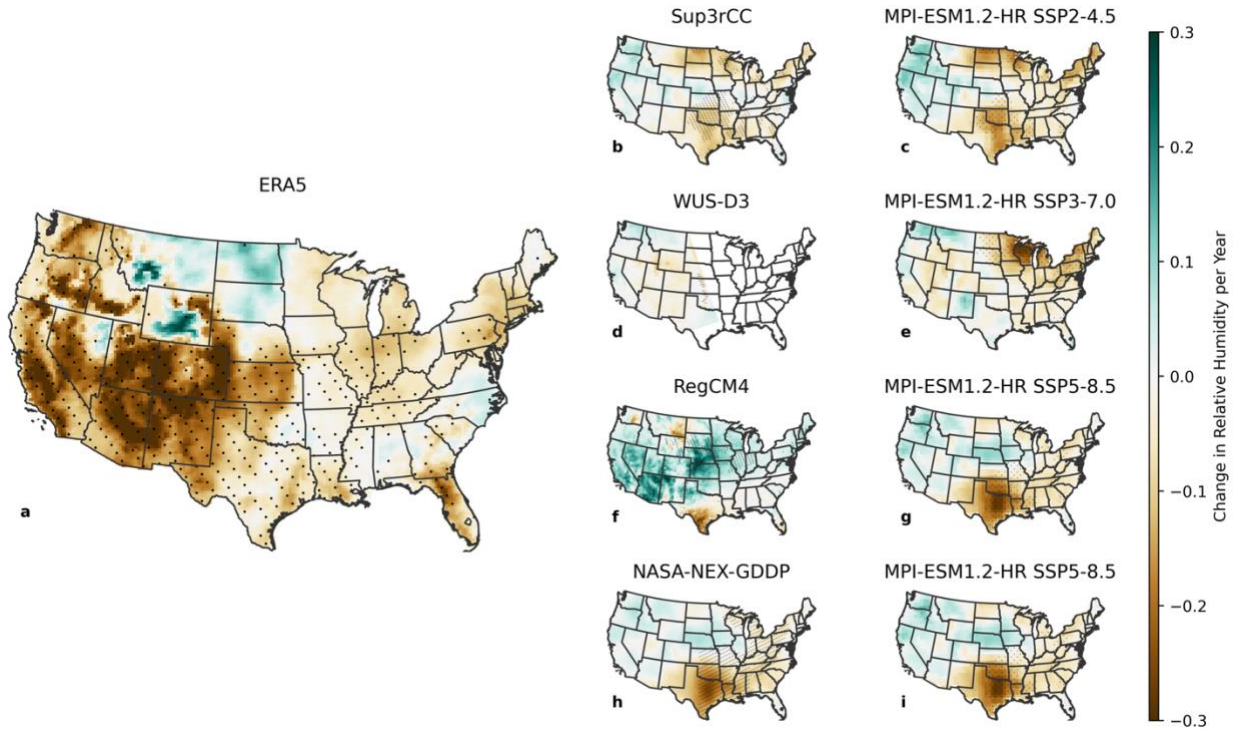

Supplementary Figure 10. Trends in 1980–2019 spring (March, April, May) near-surface relative humidity from (a) ERA5, (b, c) Sup3rCC and source ESM, (d, e) WUS-D3 and source ESM, (f, g) RegCM4 and source ESM, (h, i) NASA-NEX-GDDP and source ESM. Projections are based on the ESM MPI-ESM1.2-HR, with the "historical" CMIP6 simulation through 2014 and after 2014: SSP2-4.5 r1i1p1f1 for (b, c), SSP3-7.0 r3i1p1f1 for (d, e), and SSP5-8.5 r1i1p1f1 for (f–i). The trend was calculated in (a–e) using daily minimum relative humidity, whereas in (f–i) using daily average relative humidity. Stippling indicates statistically significant trends ($p < 0.05$).

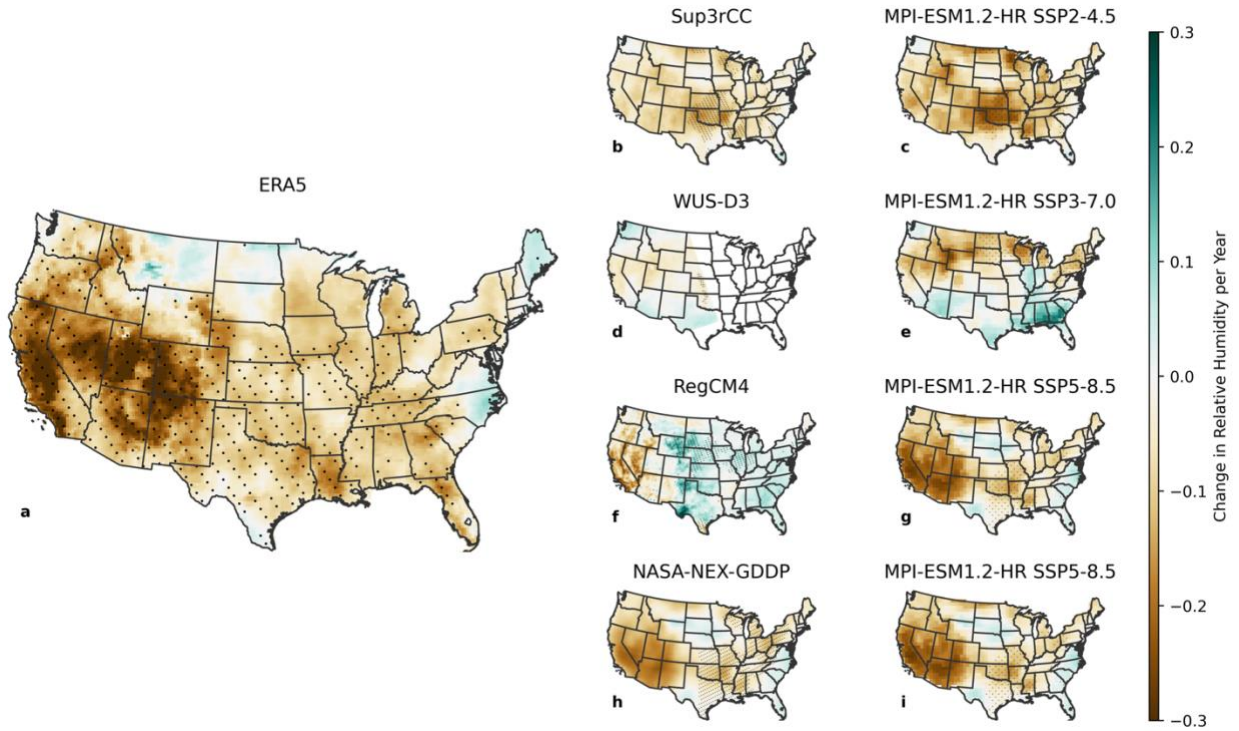

Supplementary Figure 11. Trends in 1980–2019 fall (September, October, November) near-surface relative humidity from (a) ERA5, (b, c) Sup3rCC and source ESM, (d, e) WUS-D3 and source ESM, (f, g) RegCM4 and source ESM, (h, i) NASA-NEX-GDDP and source ESM. Projections are based on the ESM MPI-ESM1.2-HR with the "historical" CMIP6 simulation through 2014 and after 2014: SSP2-4.5 r1i1p1f1 for (b, c), SSP3-7.0 r3i1p1f1 for (d, e), and SSP5-8.5 r1i1p1f1 for (f–i). The trend was calculated in (a–e) using daily minimum relative humidity, whereas in (f–i) using daily average relative humidity. Stippling indicates statistically significant trends ($p < 0.05$).

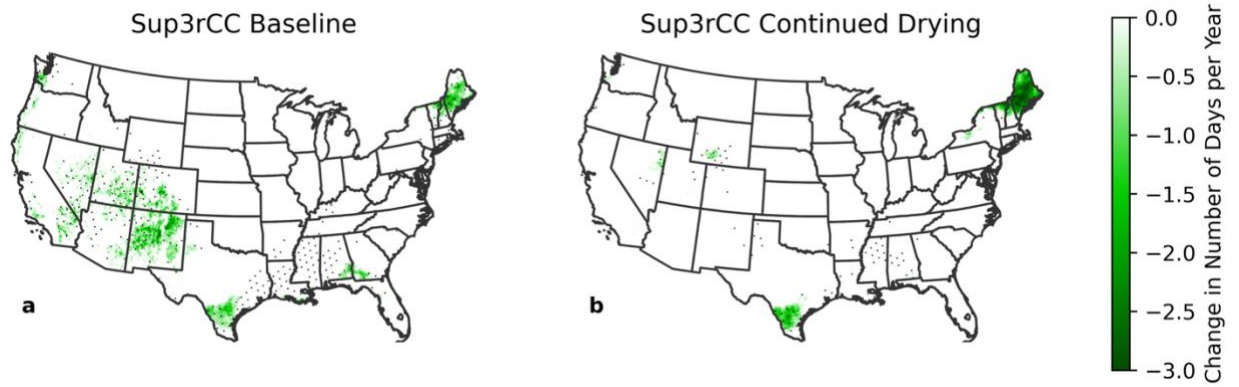

Supplementary Figure 12. Decrease in number of extreme fire weather days per year from 2000–2019 to 2020–2039 based on (a) Sup3rCC five-member ensemble and (b) continued drying scenario based on Sup3rCC five-member ensemble with trend-corrected relative humidity. Extreme fire weather days are defined as days with FWI above the 95th percentile value calculated per pixel over the 2000–2019 period. Stippling indicates where three or more ensemble members agree on a decrease in extreme FWI days and a statistically significant shift in 20-year distributions ($p < 0.05$).

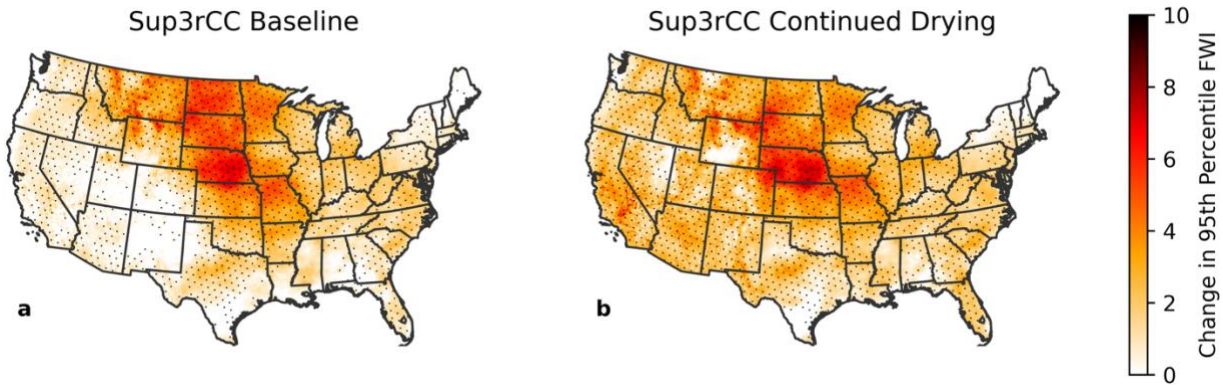

Supplementary Figure 13. Increase in the annual 95th percentile FWI from 2000–2019 to 2020–2039 based on (a) Sup3rCC five-member ensemble and (b) continued drying scenario based on Sup3rCC five-member ensemble with trend-corrected relative humidity. Stippling indicates where three or more ensemble members agree on an increase in 95th percentile FWI and a statistically significant shift in 20-year distributions ($p < 0.05$).

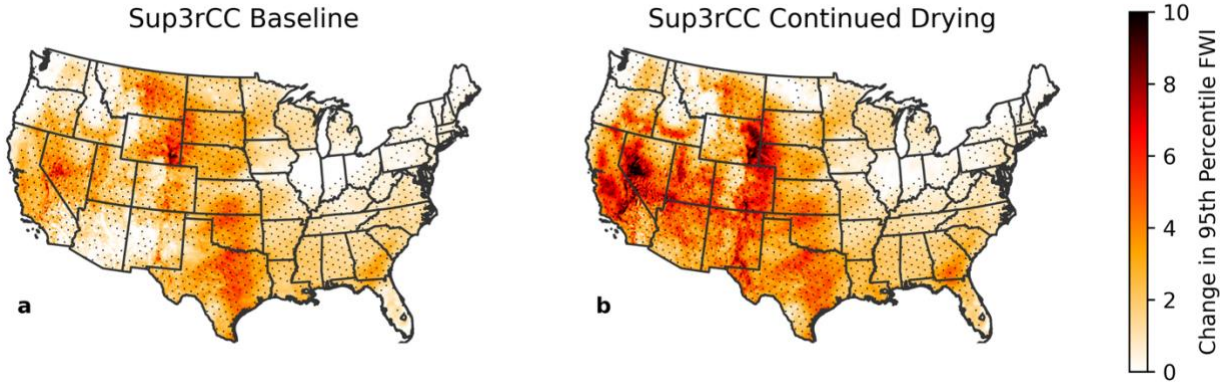

Supplementary Figure 14. Increase in the winter (December, January, February) 95th percentile FWI from 2000–2019 to 2020–2039 based on (a) Sup3rCC five-member ensemble and (b) continued drying scenario based on Sup3rCC five-member ensemble with trend-corrected relative humidity. Stippling indicates where three or more ensemble members agree on an increase in 95th percentile FWI and a statistically significant shift in 20-year distributions ($p < 0.05$).

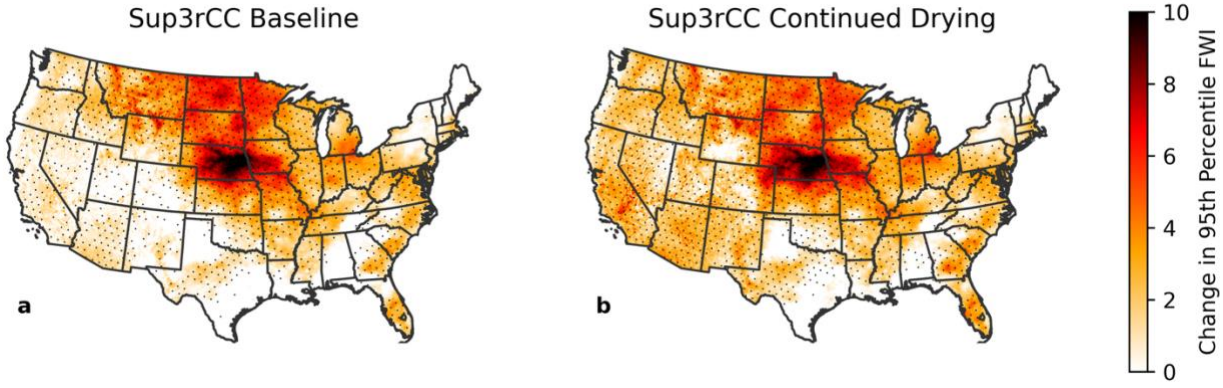

Supplementary Figure 15. Increase in the summer (June, July, August) 95th percentile FWI from 2000–2019 to 2020–2039 based on (a) Sup3rCC five-member ensemble and (b) continued drying scenario based on Sup3rCC five-member ensemble with trend-corrected relative humidity. Stippling indicates where three or more ensemble members agree on an increase in 95th percentile FWI and a statistically significant shift in 20-year distributions ($p < 0.05$).

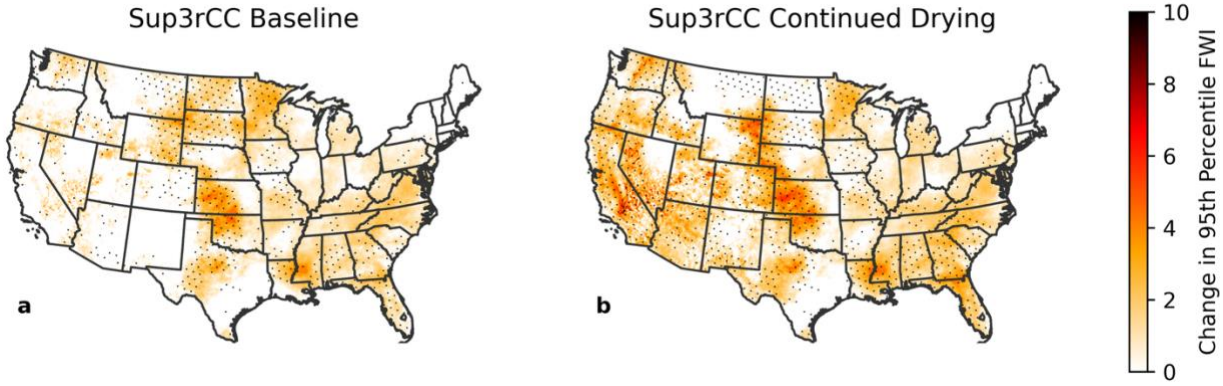

Supplementary Figure 16. Increase in the spring (March, April, May) 95th percentile FWI from 2000–2019 to 2020–2039 based on (a) Sup3rCC five-member ensemble and (b) continued drying scenario based on Sup3rCC five-member ensemble with trend-corrected relative humidity. Stippling indicates where three or more ensemble members agree on an increase in 95th percentile FWI and a statistically significant shift in 20-year distributions ($p < 0.05$).

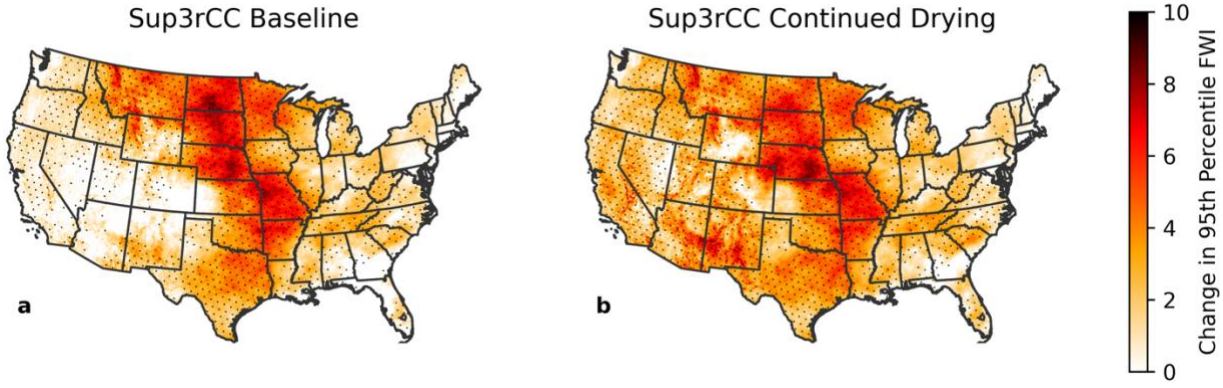

Supplementary Figure 17. Increase in the fall (September, October, November) 95th percentile FWI from 2000–2019 to 2020–2039 based on (a) Sup3rCC five-member ensemble and (b) continued drying scenario based on Sup3rCC five-member ensemble with trend-corrected relative humidity. Stippling indicates where three or more ensemble members agree on an increase in 95th percentile FWI and a statistically significant shift in 20-year distributions ($p < 0.05$).